

Interfacial Dirac Cones from Alternating Topological Invariant Superlattice Structures of Bi_2Se_3

Jung-Hwan Song,^{*} Hosub Jin, and Arthur J. Freeman*Department of Physics and Astronomy, Northwestern University, Evanston, Illinois 60208, USA*

(Received 3 June 2010; published 27 August 2010)

When the three-dimensional topological insulators Bi_2Se_3 and Bi_2Te_3 have an interface with vacuum, i.e., a surface, they show remarkable features such as topologically protected and spin-momentum locked surface states. However, for practical applications, one often requires multiple interfaces or channels rather than a single surface. Here, for the first time, we show that an interfacial and ideal Dirac cone is realized by alternating band and topological insulators. The multichannel Dirac fermions from the superlattice structures open a new way for applications such as thermoelectric and spintronics devices. Indeed, utilizing the interfacial Dirac fermions, we also demonstrate the possible power factor improvement for thermoelectric applications.

DOI: 10.1103/PhysRevLett.105.096403

PACS numbers: 71.20.-b, 73.20.At, 73.21.Cd

Newly discovered “second-generation” three-dimensional topological insulators such as Bi_2Se_3 and Bi_2Te_3 have attracted great attention due to their exceptional properties when they have a surface, i.e., relatively large bulk band gaps, and one simple Dirac cone at the Γ point in the Brillouin zone (BZ). Their surface states are protected by time-reversal symmetry and show the Dirac cones connecting the inverted conduction and valence bands [1,2]. These Dirac cones constitute the topological transport regime, which has the gapless conducting and spin-momentum locked surface states leading to the suppression of backscattering. Such extraordinary surface states of the three-dimensional topological insulators may occur, as the term “surface” already suggests, only at the surfaces or, more generally, interfaces where the topological invariant changes [3,4]. For these topological insulators, the extension of a single surface to multiple interfaces, i.e., a periodic array of alternating band and topological insulators [topological–band insulator (TI–BI) superlattices], has not been attempted yet although multiple interfacial Dirac cones in bulk led to new technological opportunities for practical applications such as thermoelectric and spintronic devices.

Here we use a first-principles density functional approach to design superlattice structures, using Bi_2Se_3 topological insulators, whose interfacial electronic structures show the Dirac cones with massless linear dispersion to be the same as a single surface state. We propose O substitutions to make the interface layers, which eventually creates the band insulator layers alternating with topological insulator layers. Advanced crystal growth techniques such as molecular beam epitaxy may be useful for achieving TI–BI superlattices suggested here, as used in recent topological insulator experiments [5]. Utilizing possible high mobilities from multiple interfacial Dirac cones, we also demonstrate the power factor improvement for thermoelectric applications.

The theoretical calculations were performed employing the highly precise full-potential linearized augmented plane

wave (FLAPW) [6,7] method with the gradient-corrected Perdew, Burke, and Ernzerhof form [8] of the exchange-correlation potential. The lattice constants and the internal atomic coordinates were fully optimized; it is assumed that O substitution does not change the in-plane lattice constants. The core states and the valence states were treated fully relativistically and scalar relativistically, respectively. For \mathbf{k} -space integrations, a $9 \times 9 \times 1$ mesh of special \mathbf{k} points was used in the irreducible Brillouin zone wedge. The energy cutoffs for the interstitial plane-wave basis and the star functions were 13.0 and 100.0 Ry, respectively. If not otherwise specified, all calculated results include spin-orbit coupling (SOC) by a second variational procedure [9]. The muffin-tin radii of Bi, Se, and O were 2.9, 2.4, and 1.5 bohr, respectively. To calculate the power factors, the Boltzmann distribution function was employed in the constant relaxation time approximation. To determine the group velocities which are used in the transport coefficients, we use full intraband optical matrix elements [10] calculated within the FLAPW method. Different carrier concentrations for the transport coefficient calculations were treated within the rigid band model.

The Bi_2Se_3 crystal has a rhombohedral unit cell or a layered structure stacked along the c axis of the hexagonal lattice, as shown as Fig. 1(a). One quintuple-layer slab has one formula unit in which the anion Se atom has two different sites. The Se atom at the center has covalent bonds with six Bi atoms, and the other Se site has three covalent bonds with Bi, but has van der Waals interactions with three Se atoms in the other quintuple-layer slab. To construct TI–BI superlattices, we use the hexagonal supercell structures whose (0001) interfaces correspond to a two-dimensional hexagonal Brillouin zone, as in the film geometry.

When we substitute O atoms for Se atoms in the van der Waals layers, O–Bi layers form band insulator layers, which leads to the interfaces between topological and band insulators, i.e., the change of the topological invariant.

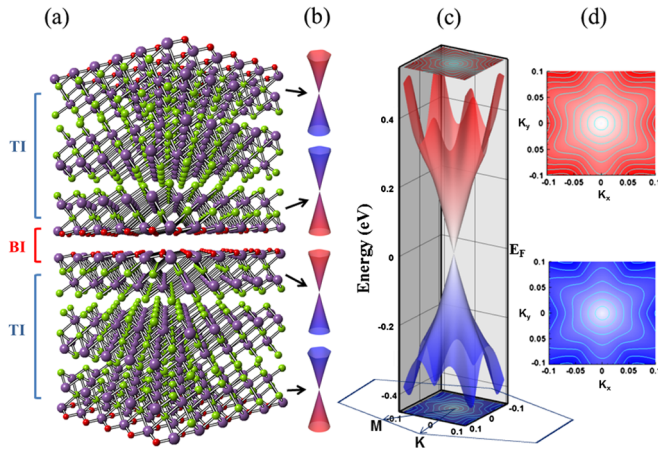


FIG. 1 (color online). (a) Superlattices of alternating band (BI) and topological (TI) insulators. (b) Dirac cones representing each interface state between the layers of band and topological insulators in (a). (c) Three-dimensional plot of the interface state of (a), and (d) its contour plot above and below the Kramers point. The contour interval is 0.05 eV.

Hence, as shown in Fig. 1(b), the “three-dimensional” systems from the superlattice structure of the alternating topologically distinct insulators give rise to a Dirac cone in the BZ for each interface just as for their surfaces. We should note that the topological transport regime from each interface is as robust in the presence of nonmagnetic impurities as that of their surface states since the backscattering is still forbidden by time-reversal symmetry.

In the pristine Bi_2Se_3 surfaces, it is known to be difficult to isolate the surface states from the bulk states especially by transport measurements [4,11]. The band structures of the pristine Bi_2Se_3 surfaces, which are confirmed by theoretical calculations [1,12], clearly show that the Kramers point is close to or even lower than the bulk valence bands, which leads to possible elastic scattering channels between the surface and bulk states. The hexagramlike isoenergy contours in the BZ far from the Kramers point, but still within the bulk band gap, also provide the finite \mathbf{q} elastic scattering channels [13], which reduces the energy range for observing the transport effects of the ideal Dirac cones.

The theoretical calculations for the Bi_2Se_3 superlattices, which are composed of three quintuple layers with O substitution at the top and bottom surfaces, show a very similar band structure to that for their film geometries; the spin-split interface states by the spin-orbit coupling traverse the bulk band gap between Kramers pairs at \mathbf{k} and $-\mathbf{k}$, and cross each other at the Γ point, resulting in the “ideal” Dirac cones.

The Dirac cones which originate from the O substitution are ideal in the topological insulators in the sense that they show a significantly improved topological spin transport regime compared to that of the pristine Bi_2Se_3 surfaces; as shown in Fig. 1(c), the Fermi level is located at the Kramers point in the middle of the bulk band gap of approximately 0.48 eV, which is relatively large compared to the bulk

Bi_2Se_3 band gap of 0.3 eV [14]. The surface states in Fig. 1(d) also show the circular isoenergy contours in the BZ within the range of 0.3 eV centered at the Kramers point. The fact that the Kramers point at the Fermi level is far away from the bulk bands is related to the role of O-Bi (band insulator). In Fig. 2(a), the charge density plot of the surface state at Γ illustrates that the surface states mostly reside in the van der Waals layers near the interface where two Se atoms face each other, not in the O-Bi layers [see Fig. 2(b)]. This fact is of great significance since the effect of possible disorders in the O-Bi layers is expected to be small on the surface states [15]. Note that, in Fig. 2(a), the Bi in the O-Bi layer has almost no contribution to the surface states, as the Se also does not at the center of three Bi_2Se_3 quintuple layers sandwiched by O.

The large bulk band gap obtained here also suggests a crucial point, i.e., a tunable bulk band gap which can be controlled by the thickness of the Bi_2Se_3 layers between the O layers. The topological insulator region in the superlattice structures barely sees (or interacts with) each other over the band insulators. The bulk band gaps in these superlattices are determined by quantum confinement, as in the film geometry. The detailed band structure for the superlattices in Fig. 2(b) shows a bulk band gap of approximately 0.59 eV in Fig. 2(c) when the SOC is not

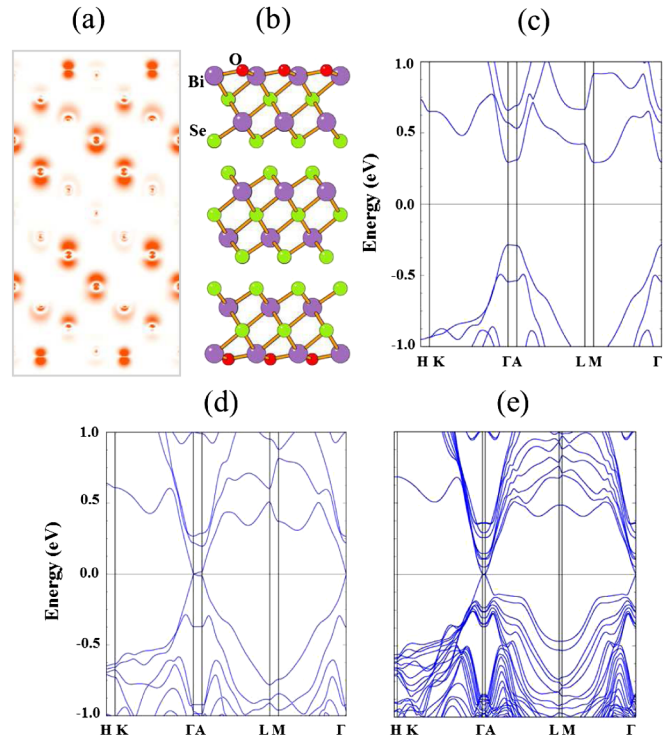


FIG. 2 (color online). (a) The charge density plot of the surface states at Γ and (b) its corresponding Bi_2Se_3 structure with O substitution at both ends, which is a periodic unit of superlattices along the c axis in Fig. 1(a). The band structures of superlattices of three quintuple layers [(c),(d)] and (e) nine quintuple layers of Bi_2Se_3 with O substitution at both ends. In (c), only the Perdew, Burke, and Ernzerhof functional is used without spin-orbit coupling (SOC), but (d) and (e) include the SOC.

included in the calculations, while the calculations with the SOC yield Dirac-cone-like interface states which originate from the distinct topological invariants between the band and topological insulators, as shown in Fig. 2(d). The thicker nine quintuple layers of topological insulators between the O layers yield nearly the same bulk band gap as that of the bulk Bi_2Se_3 [see Fig. 2(e)]. Also we note that the possible interactions between the interfaces due to a thin topological insulator slab in superlattices may result in slightly dispersive interface states along Γ to A as shown in Fig. 2(d), while the topological insulator slab which is sufficiently thick to prevent the interactions between the interfaces should give nearly flat bands, as shown in Fig. 2(e). This is an analogy to opening a gap at the Kramers point due to the intersurface interaction in ultrathin films. These results are all of importance not only for technological applications but also for observing novel phenomena driven by the helical Dirac fermions.

The optimized geometry in Fig. 2(b) shows a consistent picture with the nature of the alternating topological invariants as well. The O binds strongly with Bi and shrinks significantly towards the Bi. Their distance is only 2.4 Å, which makes nearly a perfect single layer of O and Bi. The Bi in the O-Bi layer has a slightly larger bonding distance with Se, by 0.01 Å, compared to those of other Bi-Se bonds where the Bi has only Se as a nearest neighbor, which also guides us to distinguish the band (O-Bi) and topological insulator layers.

The Bi-based chalcogenides such as Bi_2Se_3 and Bi_2Te_3 are typical materials for thermoelectric applications due to their relatively low thermal conductivities. As illustrated above, the O substitution in the Bi_2Se_3 gives the ideal transport regime for Dirac fermions, as well as the high density of the interfacial Dirac cones in the superlattice structures. These facts naturally lead us to the investigation of possible improvements for thermoelectric applications. The performance of the thermoelectric materials is determined by the figure of merit, $ZT = S^2\sigma T / (\kappa_e + \kappa_L)$, where S is the Seebeck coefficient, σ is the electrical conductivity, and κ_e and κ_L are the electronic and lattice thermal conductivities, respectively.

The ideal Dirac transport regime may result in as high mobilities as the graphene systems, especially by suppressing the scattering channels as discussed above, and the high density of the interfacial Dirac cones yields a high carrier concentration. In graphene, Dirac fermions are known to exhibit ballisticlike transport depending on the experimental conditions; the mobilities of the charge carriers in graphene can easily exceed $15\,000\text{ cm}^2\text{ V}^{-1}\text{ s}^{-1}$, and even reach $100\,000\text{ cm}^2\text{ V}^{-1}\text{ s}^{-1}$ in a suspended graphene [16]. The observed high mobilities in graphene show a weak dependence on temperature ($<300\text{ K}$) indicating impurities as a dominant source of scattering, and remain high even at high carrier concentration ($>10^{12}\text{ cm}^{-2}$) regardless of the doping methods [17]. Moreover, the interfacial Dirac cones from the three-dimensional topological insulators retain several advantages over graphene for high mobilities.

Apparently absent in the superlattice systems studied here are the interactions between graphene and the substrate, microscopic inhomogeneity (graphene sheet's warping and rippling), and possible elastic scattering channels due to the double spin and double valley degeneracy of the graphene's Dirac cones, which affect conductivities adversely.

To investigate the possible improvements in the power factor ($S^2\sigma$), we calculate S and σ by employing the Boltzmann distribution function in the constant relaxation time approximation [10]. We focus here on the low temperatures ($<200\text{ K}$) considering several strong and weak points. The electronic contribution to the thermal conductivity can be suppressed by the low temperature. The mobilities may tend to remain high at low temperatures by subduing phonon contributions as in the graphene systems. The gapless feature yields reduced Seebeck coefficients at high temperatures due to thermal excitation. Assuming $10\,000\text{ cm}^2\text{ V}^{-1}\text{ s}^{-1}$ for mobilities, which is smaller by a factor of 10 than the reported maximum value for graphene, the calculated power factors in the superlattice of Fig. 3(a) still show significantly larger values by a factor of approximately 10 for p type at 200 K than those observed in the Bi_2Se_3 single crystals [18]. Figure 3(a) shows the power factors only for shallow chemical potentials within the Dirac transport regime to avoid the bulk states. The unusual increase in the Seebeck coefficients in Fig. 3(b) when the chemical potentials are very deep (e.g., $\sim 0.2\text{ eV}$ below the Kramers point at 100 K) originates from the contribution of the bulk valence bands. However, the possible multiple scattering channels at these deep chemical potentials may reduce the relaxation time and thus mobilities significantly.

To suppress the lattice thermal conductivities, but to maintain the high conductivities of the interfacial Dirac fermions, the scattering centers (or layers) for phonons can be introduced in the band or topological insulator layers far from the interface. This phonon-blocking and electron-transmitting strategy is well known for thermoelectric studies, as can be found in $\text{Bi}_2\text{Te}_3/\text{Sb}_2\text{Te}_3$ experiments [19]. In this context, we introduce thin Sb_2Se_3 layers in the Bi_2Se_3 topological insulator layers as shown in Fig. 4(a). Even though Sb_2Se_3 bulk is known as a band insulator, as shown in Fig. 4(b), introducing thin Sb_2Se_3 layers in the layers of the Bi_2Se_3 does not make another discontinuity of a topological invariant, and thus shows Dirac cones only at the

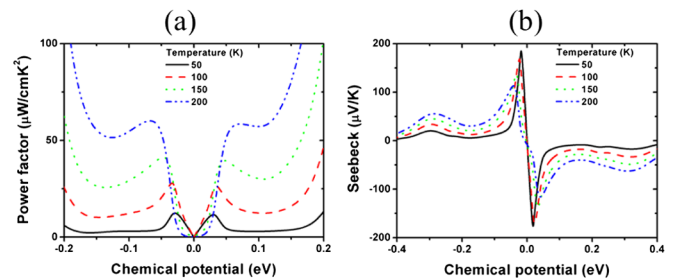


FIG. 3 (color online). (a) Calculated power factors and (b) Seebeck coefficients of superlattices in Fig. 1(a).

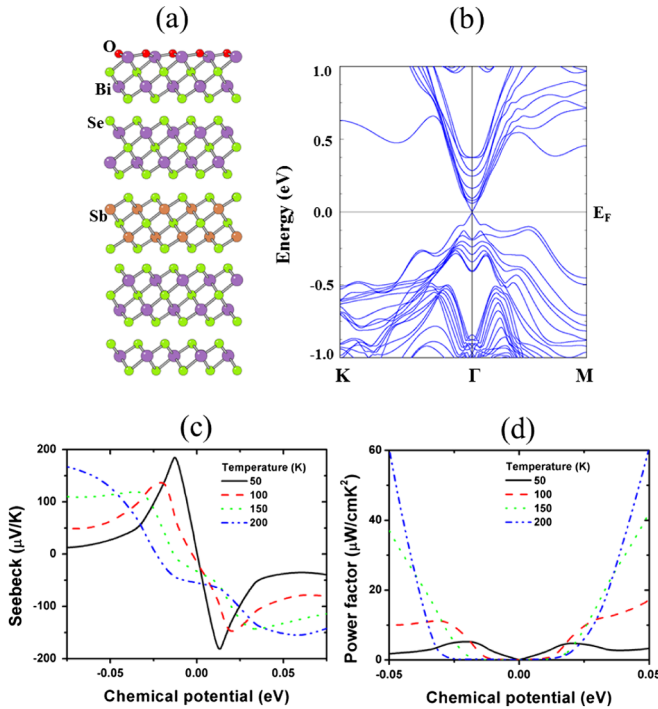


FIG. 4 (color online). (a) $\text{Bi}_2\text{Se}_3/\text{Sb}_2\text{Se}_3$ superlattices with O substitution at the top end, which is the upper half of a periodic unit along the c axis. The lower half has an inversion symmetry. (b) The band structure, (c) calculated Seebeck coefficients, and (d) power factors of superlattices in (a).

interface with the O-Bi layers as before. The bulk band gap in Fig. 4(b) is approximately 0.15 eV, mainly due to the thick (nine quintuple) layers of the topological insulators between the O layers. As shown in Fig. 4(c), this small bulk band gap significantly affects Seebeck coefficients which show n -type dominating behavior for relatively high temperatures (>150 K) due to the high density of states in the conduction bands near the Kramers point. With the band gap effect, the low density of the interfacial Dirac cones in the superlattices of the thick nine Bi_2Se_3 quintuple layers gives rise to the relatively smaller power factors in Fig. 4(d) compared to those of three Bi_2Se_3 quintuple cases in Fig. 3(a). This illustration clearly shows the possibility of manipulating the phononic contribution as well as the bulk band gaps, which makes it important to find the optimal thicknesses for band and topological insulators; inserting extra layers (as Sb_2Se_3 in this case) to reduce the thermal conductivities may possibly give a smaller bulk band gap and a lower density of the interfacial Dirac cones. In addition, the tuning of the chemical potential within the Dirac transport regime will be limited by the bulk band gap.

Inserting magnetic layers near the interface of the superlattices will open a gap at the Γ point by applying a local magnetic field to the interface and breaking local time-reversal symmetry. The nonzero gap at the Kramers point will play an important role in determining the Seebeck coefficients, which should be investigated in the future not only for the thermoelectrics but also for other applications such as spintronics.

The O substitution in the topological Bi_2Se_3 insulators yield not only the interfacial Dirac cones from the alternating different topological invariants, but also the ideal topological transport regime. This will open new technological opportunities with their long coherent length, high mobilities, and high densities of the interfacial helical Dirac fermions. The understanding of such a remarkable structure sheds light on designing thermoelectric and spintronics applications.

Financial support from the U.S. DOE under Grant No. DE-FG02-88ER45372 is gratefully acknowledged.

*jhsong@pluto.phys.northwestern.edu

- [1] Y. Xia *et al.*, *Nature Phys.* **5**, 398 (2009).
- [2] H. Zhang *et al.*, *Nature Phys.* **5**, 438 (2009).
- [3] L. Fu, C.L. Kane, and E.J. Mele, *Phys. Rev. Lett.* **98**, 106803 (2007).
- [4] M. G. Hasan and C.L. Kane, *arXiv:1002.3895* [Rev. Mod. Phys. (to be published)].
- [5] Y. Zhang *et al.*, *arXiv:0911.3706*.
- [6] E. Wimmer, H. Krakauer, M. Weinert, and A.J. Freeman, *Phys. Rev. B* **24**, 864 (1981).
- [7] H.J.F. Jansen and A.J. Freeman, *Phys. Rev. B* **30**, 561 (1984).
- [8] J.P. Perdew, K. Burke, and M. Ernzerhof, *Phys. Rev. Lett.* **77**, 3865 (1996).
- [9] A.H. MacDonald, W.E. Pickett, and D.D. Koelling, *J. Phys. C* **13**, 2675 (1980).
- [10] M.S. Park *et al.*, *Phys. Rev. B* **81**, 155211 (2010).
- [11] J.E. Moore, *Nature (London)* **464**, 194 (2010).
- [12] W. Zhang, R. Yu, H.-J. Zhang, X. Dai, and Z. Fang, *arXiv:1003.5082*.
- [13] Z. Alpichshev *et al.*, *Phys. Rev. Lett.* **104**, 016401 (2010).
- [14] A Kohn-Sham density functional scheme with the local density approximation usually yields underestimated band gaps. Hence, the calculated large band gaps are mainly due to quantum confinement effects as explained in the text. However, the local density approximation for Bi_2Se_3 bulk is known to give a relatively good estimate for the band gap, 0.3 eV, only 0.05 eV smaller than the measured one (Ref. [1]).
- [15] The optimized geometry gives an approximately 2% larger distance between Se-Se van der Waals (vdW) bound layers than the experimental value. The small possible error for the optimized O-O vdW layer distances due to the Perdew-Burke-Ernzerhof functional should have little effect on the interface states since, as explained in the text, the interface states mostly reside in the Se-Se vdW layers near the interface, but not in the band insulator (O-Bi) region nor in the O-O vdW layers.
- [16] X. Du, I. Skachko, A. Barker, and E.Y. Andrei, *Nature Nanotech.* **3**, 491 (2008).
- [17] A.K. Geim and K.S. Novoselov, *Nature Mater.* **6**, 183 (2007).
- [18] Y.S. Hor *et al.*, *Phys. Rev. B* **79**, 195208 (2009).
- [19] R. Venkatasubramanian, E. Siivola, T. Colpitts, and B. O'Quinn, *Nature (London)* **413**, 597 (2001).